Magnetic chargeability

Marcos A.R. Tschoepke* (AFC Geofísica), Antonio F.U. Costa (AFC Geofísica)

Abstract

This paper analyzes the effect of the massive presence of a high magnetic material as magnetite on the Time-Domain Induced Polarization (TDIP) surveys. A RLC electrical circuit model of the half-space is used to contribute to the interpretation. The results confirmed how the presence of a high magnetic permeability material in the medium can produce negative chargeability values.

Introduction

Negative chargeability values have been assigned to the noise caused by inductive coupling or even by the geometrical arrangement of the electrodes (Sumner, 1976; Loeb and Bertin, 1976). In general, the negative IP in the geophysical literature is not considered a physical effect, i. e. an intrinsic physical property of earth materials. However, Nabighian and Elliot (1976) relates negative chargeability to subhorizontal layers K-type ($\rho1 < \rho2 > \rho3$) and Q ($\rho1 > \rho2 > \rho3$). Hohmann (1982) related the negative values to the 2-D and 3-D bodies. Brandes and Acworth (2003) related the negative chargeability values to the clay-rich lithology such as thick sediments in coastal deposits. A very recent paper, (Patella, 2008), demonstrated that in certain situations, negative chargeability values can be explained as an intrinsic physical property in specific field cases, usually associated to the presence of hydrocarbons. This paper presents a situation where the chargeability may be negative due to the massive presence of a high magnetic permeability material on a half-space. In this case the energy stored in a magnetic field creates a condition for the existence of a negative chargeability, which we called "magnetic chargeability".

Theoretical fundaments

Description of the half-space

Figure 1 illustrates the structure of a half-space and shows the resistivity regions ρ_1, ρ_2, ρ_3 the magnetic permeability μ_1, μ_2, μ_3 and indicates the TDIP survey. Consider that the distance between the electrodes AB is much larger than thickness of the layers; $\rho_2 << \rho_3 << \rho_1$; $\mu_1 << \mu_2 >> \mu_3$ i.e. the rectangular block consists of conductive material of high magnetic permeability.
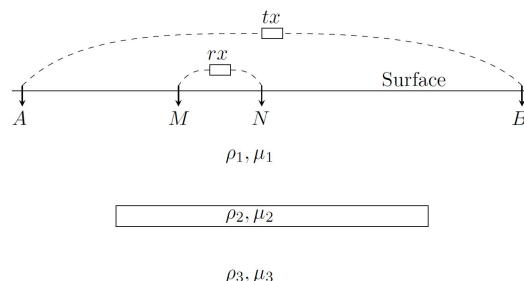

Figure 1: Half-space representation

Electric current density

The distribution of electrical current density applied on the ground by the IP transmitter tx is concentrated where resistivity ρ is low, and flow is sparse where resistivity is higher (Telford et al., 1976).

Figure 2 illustrates the current distribution flow after a transient period.
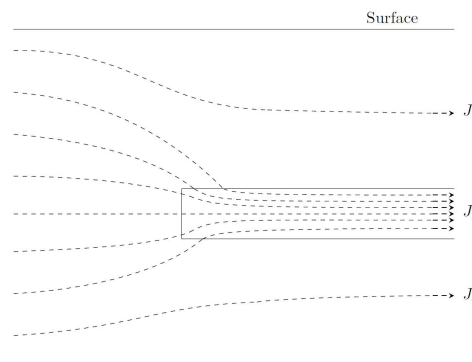

Figure 2: Electrical current flowing in the layered half-space

Magnetic field

Consider the buried conductive body large enough to take a volumetric cut concentration in a zone where the current flow converges as illustrated in Figure 3.

Figure 4 illustrates the electric current distribution flowing in a half-space region where the high concentration is observed in the conducting body.
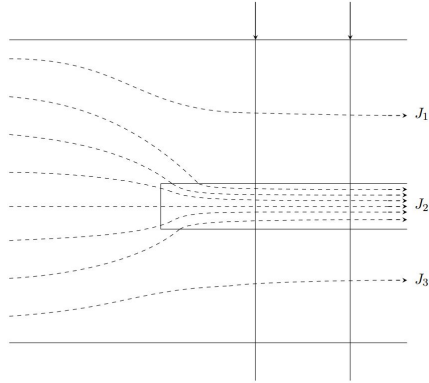
Figure 3: Half-space cut

According to Ampere's law, equations (1) and (2),the magnetic field **H** is much higher in the conductive body due to the higher current density and high magnetic permeability compared with other zones.
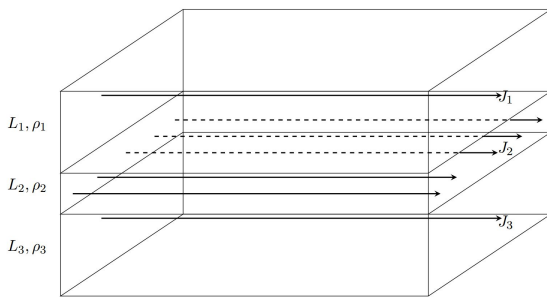

Figure 4: Volumetric cut

After the transient response time, the electric field became constant. So, we can consider the Ampère's law - equations (1) and (2), without the displacement current term.

$$\nabla \times \mathbf{H} = \mathbf{J} \qquad (1)$$

$$\oint_C \mathbf{H} \cdot d\mathbf{l} = \int_S \mathbf{J} \cdot d\mathbf{S} \qquad (2)$$

Considering that the current inside the conductive body is much higher and the magnetic permeability of the conductive body is equally high compared to other half-space regions, we can disregard the magnetic field outside the conductive body.

Magnetic field in a conductor of rectangular cross section

Holloway and Kuester (2009) studied the magnetic field distribution in a conductor of rectangular cross section and developed equations to define the magnetic field within the conductor. The results were applied to calculate the magnetic field within the conductive body.

Figures 5, 6 and 7 illustrate the magnetic fields inside the

conductive body during the on state of the IP transmitter in an instant time after the transient response.
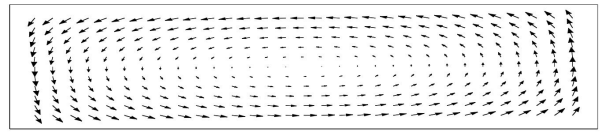

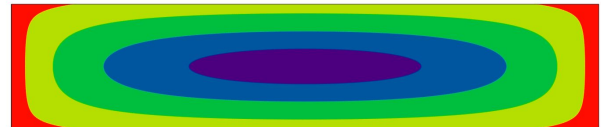Figure 5: Vector field **H** in a cross section of the conductive body

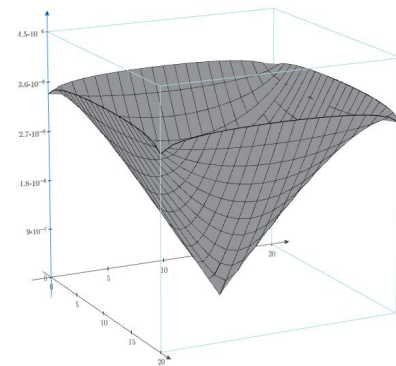Figure 6: **H** intensity in a cross section conductive body

Figure 7: **H** Intensity in a 3D field representation

Magnetic field response

Our interest in Induced Polarization is the response after the current has been cut off determined by Faraday's law, equation (3) or the integral form, equation (4).

$$\nabla \times \mathbf{E} = -\mu \frac{\partial \mathbf{H}}{\partial t} \qquad (3)$$

$$\oint_C \mathbf{E} \cdot d\mathbf{l} = -\mu \frac{d}{dt} \int_S \mathbf{H} \cdot d\mathbf{S} \qquad (4)$$

According to Faraday's Law, equation (3), after the current cut off, the magnetic field decay generates an electric field as illustrated in Figure 8. The generated electric field acts to keep the current flowing, Figure 9, and the magnetic field constant.

After the current transmitter has been turned off, the energy, U, storage in the magnetic field, equation (5), is dissipated in the medium surrounding the magnetic body, equation (6).
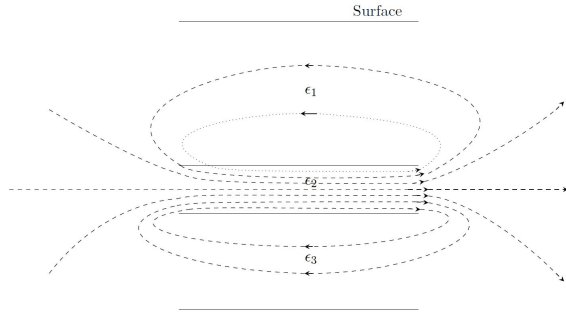
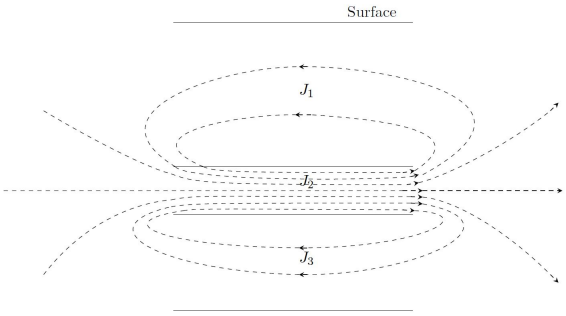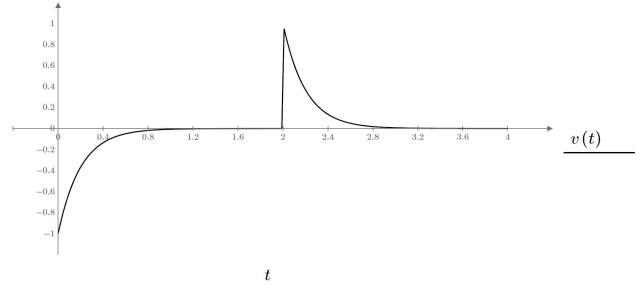Figure 8: Electric field after the transmitter cut off

Figure 10: Voltage response on magnetic medium

transmitter and response resulting from the decay magnetic field after the current cut off, equation (7).
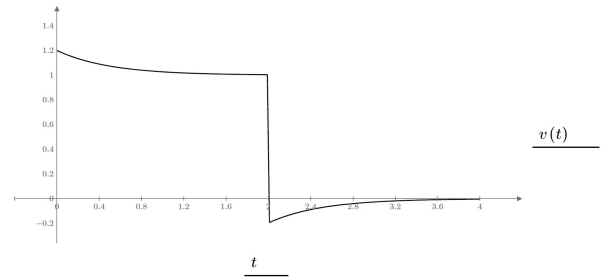

Figure 9: Current circulation after the transmitter cut off

Figure 11: IP signal measured in MN

Simulation of RL electrical circuit model

RL circuit model

This section presents a simplified model, which considers only the magnetic field (inductive). The following section includes the response of the electric field (capacitive).

Figure 12 illustrates a circuit model for the half-space considered in Figure 1.
The magnetic body is replaced by an inductor L_m and a resistor R_m.

$$U = \frac{\mu}{2} \int_V \mathbf{H} \cdot \mathbf{H} dV \tag{5}$$

$$U = R \int_{t1}^{t2} i(t)^2 dt \tag{6}$$

Considering the conductive body immersed in a purely resistive and homogeneous medium, the equations (7) and (8) show the voltage $v(t)$, Figure 10, and current $i(t)$ on the conductive body after the transmitter has been cut off, determined by the equation (3).

$$v(t) = -V_0 e^{-\frac{1}{\tau}t} \tag{7}$$

$$i(t) = I_0 e^{-\frac{1}{\tau}t} \tag{8}$$

Where τ is a constant determined by the characteristics of the medium: dimension, magnetic permeability and resistivity.

IP response

Considering the test illustrated in Figure 1, during the on-time positive pulse of the IP transmitter the current flows from M to N, Figure 2. During the off-time the current flows from N to M, Figure 9, generating a reverse polarity voltage.

The signal measured in MN is illustrated in Figure 11, resulting from the application of the current pulse by the IP
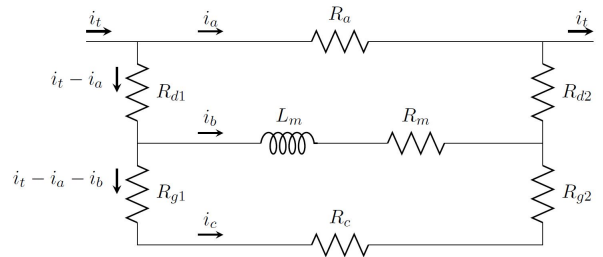

Figure 12: RL circuit model

Equivalent Inductor

The inductor value in the equivalent circuit model may be estimated using the equation developed by Holloway and Kuester (2009). The value depends on the geometric variables and magnetic permeability μ of the magnetic medium,

where $\mu = \mu_r \mu_0$ being μ_0 the magnetic permeability of free space and μ_r the relative magnetic permeability.

The relative magnetic permeability is related to magnetic susceptibility by (9):

$$\mu_r = (1 + 4\pi\kappa) \qquad (9)$$

Where κ is the magnetic susceptibility in CGS system and 4π is a constant conversion for SI (International System). To calculate the equivalent inductor let's assume that the magnetic body is an ore with a high percentage of magnetite in its composition. The magnetite magnetic susceptibility is the highest known among ores, the values presented in the literature vary, depending on the magnetite percentage in the ore (Nabighian, 1988; Telford et al., 1976).

According to Grant and West (1965), the susceptibility of magnetite ore can be calculated by equation (10).

$$\kappa = 12.2 f^{1.2} \qquad (10)$$

Where f is the magnetite percentage in the ore.

For the simulation of the circuit model, we considered a magnetic body with 55% of magnetite.

Applying the relations (9) and (10) result in a relative magnetic permeability $\mu_r \approx 76$.

For a magnetic body with arbitrary dimensions 40m wide, 40m deep and 500m long and relative magnetic permeability 76, the inductance resultant is about $1800 \mu H$ (Holloway and Kuester, 2009).

We will also consider that the medium surrounding the magnetic body consists of low resistivity material further much larger than the resistivity of the magnetic body in a manner that we can consider the circuit resistance low.

Circuit model simulation

The circuit illustrated in Figure 13 shows the model used in the simulator considering the estimated values of resistance and inductor. A current pulse of 1 Ampere is applied during the first two seconds and turned off after this time.
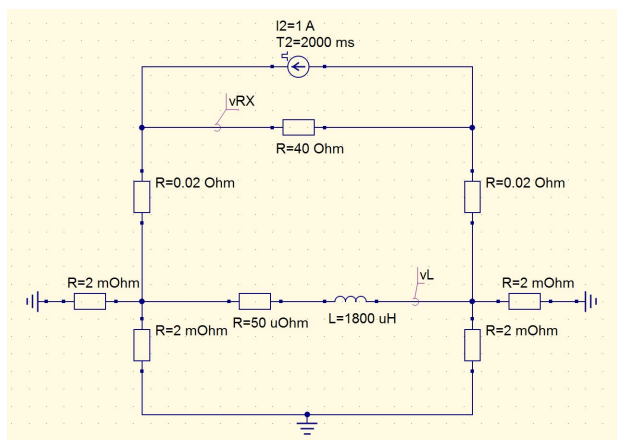

Figure 13: Simulated RL circuit model

The graphics of Figures 14 and 15, illustrate the simulation results. The nodes marked with vL and vRX are the monitoring points. The vL node corresponds to the signal resulting from the edge of the magnetic body (inductor). The vRX node corresponds to the signal observed in the surface by an IP signal receiver.
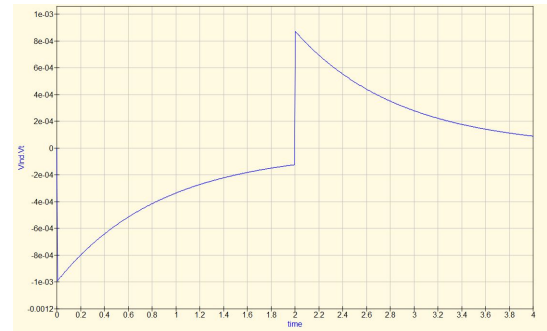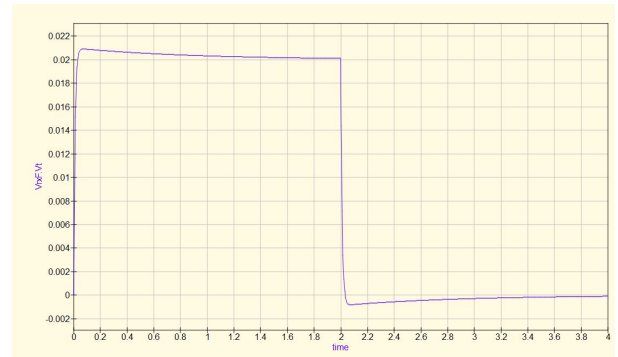

Figure 14: Signal across the inductor

Figure 15: IP receiver signal

Electric and magnetic combined IP

RLC circuit model

The model considered in the analysis above has been simplified to include only the magnetic inductive response. However, in nature, there will be also the response of the electric field, which is usually considered in the IP surveys, as illustrated in Figure 16.
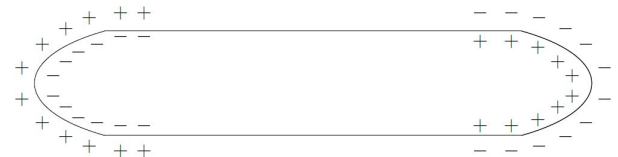

Figure 16: Electrical polarization on the surface of the conductive body

As a result, the capacitive effect will be represented in the RLC circuit model as illustrated in Figure 17.
Marshall and Madden (1959) presents capacitance and resistance values per unit area for the magnetite, which were used as a reference to estimate the approximate values of the capacitor C_e and resistor R_1 of the RLC model.
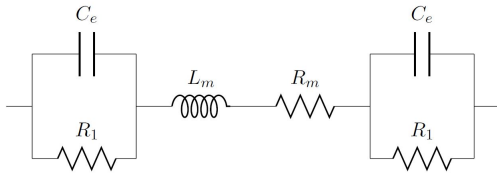
Figure 17: Equivalent RLC circuit

RLC circuit simulation

The circuit model of Figure 18 includes the IP electric and magnetic effects.
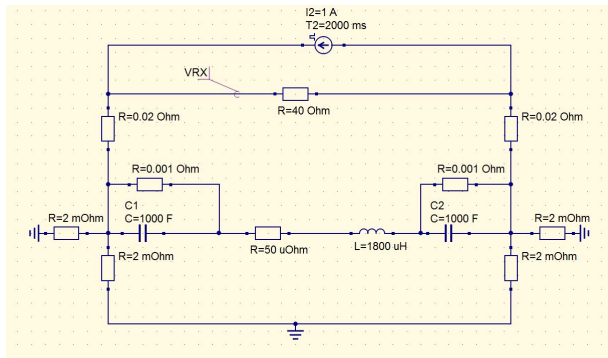

Figure 18: Simulated RLC circuit model

This circuit was simulated for two magnetic permeability values of the magnetic conductive body. The first one, illustrated in Figure 19, was considered a high relative magnetic permeability value, which results in a high inductor value. In this case the magnetic effect is predominant and the chargeability is negative. At the second one, Figure 20, was considered a low relative magnetic permeability resulting in an inductor L of low value. In this case the electric IP is predominant and chargeability is positive.

Figure 19: RLC circuit response $L = 1800\mu H$

Conclusion

The arguments presented in this paper demonstrate that negative chargeability values can be related to the massive
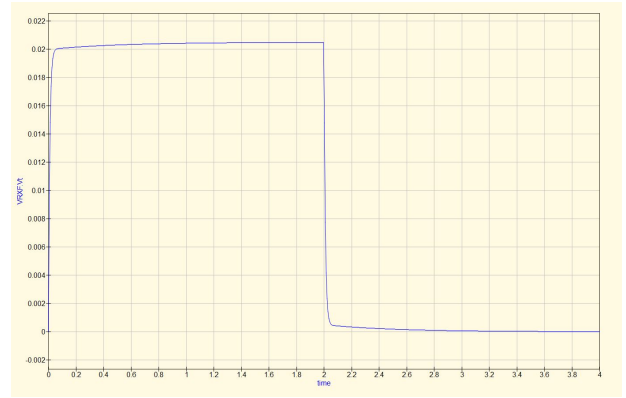

Figure 20: RLC circuit response $L = 30\mu H$

presence of conductive material of high magnetic permeability. Furthermore the medium surrounding the conductive magnetic body must be of low resistivity such that the circuit resistance is low. Otherwise the effect will not last longer enough to be measured. If the resistance is high, the energy stored in the magnetic field will be dissipated quickly.

References

Brandes, I., and Acworth, R. I., 2003, Intrinsic negative chargeability of soft clays: ASEG Extended Abstracts, **2003**, no. 2, 1–4.

Grant, F. S., and West, G. F., 1965, Interpretation theory in applied geophysics:.

Hohmann, G. W., 1982, Numerical modeling for electrical geophysical methods: Numerical modeling for electrical geophysical methods:, Proc. Int. Symp. Appl. Geophys. Trop. Reg., Belem, Braz, 308–384.

Holloway, C. L., and Kuester, E. F., 2009, Dc internal inductance for a conductor of rectangular cross section: Electromagnetic Compatibility, IEEE Transactions on, **51**, no. 2, 338–344.

Loeb, J., and Bertin, J., 1976, Experimental and theoretical aspects of induced polarization: Borntraeger.

Marshall, D. J., and Madden, T. R., 1959, Induced polarization, a study of its causes: Geophysics, **24**, no. 4, 790–816.

Nabighian, M. N., and Elliot, C. L., 1976, Negative induced-polarization effects from layered media: Geophysics, **41**, no. 6, 1236–1255.

Nabighian, M. N., 1988, Electromagnetic methods in applied geophysics: Application (2 vols.):, number 3 SEG Books.

Patella, D., 2008, Modeling electrical dispersion phenomena in earth materials: Annals of Geophysics.

Sumner, J., 1976, Principles of induced polarization for geophysical exploration:.

Telford, W., Geldart, L., and Sheriff, R. E. Keys, da, 1976 applied geophysics:, 1976.